ELSEVIER

Polymer 42 (2001) 5937–5946

polymer

www.elsevier.nl/locate/polymer

Structure–property relation in poly(*p*-phenylene terephthalamide) (PPTA) fibers

Y. Rao, A.J. Waddon, R.J. Farris*

Polymer Science and Engineering Department, Silvio O. Conte National Center for Polymer Research, University of Massachusetts at Amherst, Amherst, MA 01003, USA

Received 1 May 2000; received in revised form 1 December 2000; accepted 6 December 2000

Abstract

Structure parameters of various poly(*p*-phenylene terephthalamide fibers have been investigated using WAXD and correlated with mechanical properties. The mechanical properties examined were modulus E and strength σ; the pertinent structural parameters include orientation angle ϕ_{200}, lattice constants a, b, c, paracrystalline parameter g_{II},apparent crystal sizes ACS_{110}, ACS_{200}, ACS_{001}, intensity ratio I_{110}/I_{200} and transverse crystallinity X. The parameters, c, g_{II} and I_{110}/I_{200} are found to be interrelated and to provide indications of nonreversible chain conformational changes due to post-treatment. It is concluded that the fiber modulus is determined by the combination of the orientation of the crystallites and the paracrystalline parameter through the following equation:

$$1/E_f = (1/E_0 + D_1 g_{II}^2) + A\langle \sin^2 \phi \rangle \quad (10)$$

in which E_f is the fiber modulus; g_{II} the paracrystalline parameter; ϕ the orientation angle; and E_0, D_1 and A the material constants. This relationship is derived from our proposed morphological model in which crystallites are: (a) formed from chains have nonlinear conformations; and (b) packed with an orientation distribution. The correlation of structure with strength has also been studied. In addition, different types of Kevlar® fibers, Kevlar® 119, Kevlar® 29, Kevlar® 49 and Kevlar® 149 show slight, systematic, variations in structure. In particular, all Kevlar® fibers except Kevlar® 149 show the forbidden 001 diffraction reflection, which has been related to conformational differences.

Keywords: Poly(*p*-phenylene terephthalamide) Kevlar® fibers; Structure–property relation; Wide-angle X-ray diffraction

1. Introduction

The discovery of the poly(*p*-phenylene terephthalamide) (PPTA) fiber in 1972 brought much excitement to the polymer field [1]. Its high performance permits a wide range of applications in fiber-reinforced composites, cables and ropes, ballistic fabrics and pulps [2]. Its excellent properties continue to draw interest in the area of structure–property relationships [3–6]. However, the appearance of new types of Kevlar® fiber, especially Kevlar® 149, challenges the universal applicability of these relationships. Through a study of numerous samples of different types of Kevlar® fibers subjected to a wide variety of treatments, this paper aims to shed new light on the issue and to derive a comprehensive structure–property relationship which reconciles some of the conflicting results of previous studies.

Much work has been invested in the determination of the structure of PPTA [5,7–14]. PPTA is, of course, a highly crystalline polymer. Although the crystallinity of Kevlar® 29 fiber is 68% according to Hindeleh's measurement [5], a single-phase crystalline structure with lattice imperfections describes its morphology better [10]. The crystal structure of PPTA has been shown by Northolt and Aartsen to be pseudo-orthorhombic [7,8]. Panar and coworkers suggested a paracrystalline structure for the crystal with a second order distortion g_{II} of 2.5% along the *c*-axis [10]. Inter-molecular hydrogen bonding between the C=O and the N–H groups of the amide unit leads to the formation of hydrogen bonded sheets within the *bc* plane. These imperfect crystals pack to form pleated sheets and these pleats can be observed using polarized optical microscopy, the pleats being perpendicular to the fiber axis. Transmission electron microscopy and micro X-ray diffraction measurements showed that pleated sheets are formed in the hydrogen-bond plane and are arranged radially [12–14]. Finally, a fibrillar structure is formed. A skin-core morphology is also common due to processing [15]. In order to achieve good properties, the

* Corresponding author. Tel.: +1-413-577-3125; fax: +1-413-545-0082.
E-mail address: rjfarris@polysci.umass.edu (R.J. Farris).

0032-3861/01/$ - see front matter © 2001 Elsevier Science Ltd. All rights reserved.
PII: S0032-3861(00)00905-8

spinning and post-treatment stages are crucial. The properties of PPTA fibers have been shown to be sensitive to the temperature and tension in post-treatment [6,9,16,17].

In a structure–property relationship study, using a single-phase structural model, Northolt and Aartsen first proposed that the fiber compliance changes with the mis-orientation angle according to [3]:

$$S_{33} = e_3^{-1} + A\langle \sin^2 \phi \rangle + B\langle \sin^4 \phi \rangle$$

in which, S_{33} is the fiber compliance along the fiber axis; e_3 the crystal modulus along c-direction; and ϕ the orientation angle of crystals. On the other hand, independently, Barton showed a good correlation between the modulus and the paracrystalline parameter [4]. However, after a thermal annealing and aging study, Hindeleh and Abdo concluded that the fiber modulus increases with increasing crystallinity, although strength and elongation decrease [5]. Recently, Lee and co-authors post-treated Kevlar® fibers under different temperatures and tensions and carried out mechanical testing and X-ray measurements. Their experimental results illustrated a relation between the modulus and the orientation function and the removal of pleats. Meanwhile other structural features (paracrystalline parameter, axial and transverse crystallite sizes) were found not to dominate the material stiffness [6]. While there have been a number of studies on modulus–structure relationships, similar studies on strength–structure correlations have been rare. However, Allen and coworkers have concluded that the tensile strength of PPTA fibers is determined by the orientation and the strength anisotropy in the polymer [18]. The fiber patentees of DuPont suggest that the perfection of the radial arrangement is responsible for improved tenacity [19].

From the above it is clear that studies on structure–property relationships have led to differing conclusions amongst authors. We are of the opinion that this is because different workers have focused on specific structure parameters exclusively without due consideration for other structural parameters. Therefore, in this contribution, structure–property relationships were re-examined through a "full mapping" approach. In our experiment, the properties and structures of a wide range of as-spun fibers were changed greatly by subjecting them to different treatment conditions including different temperature, tension and hydrostatic pressure with inert gas or water. Then, the properties and structure of the modified fibers were carefully measured and all relative structure parameters were investigated.

Our experimental results strongly indicate the modulus of the fiber is determined by the combination of the mis-orientation and the paracrystalline parameter. This can be thought of as a combination of macro orientation (conventional orientation of a fiber) and local orientation (chain linearity within a crystallite). A morphological model has been proposed and provides good agreement with experimental results.

2. Experimental

Kevlar® 119, Kevlar® 29, Kevlar® 49 and Kevlar® 149 fibers were supplied by DuPont. These four different fibers were subjected to different post-treatment conditions described elsewhere [20]. After different treatments, their mechanical properties and structure were characterized.

In order to improve the statistical analysis of the results, multi-filament yarn specimens were used for mechanical property tests. Single filament tests were used only when yarn samples were not available. Five repeat tests were performed for yarn specimens and ten for single filaments. The tensile testing of yarn specimens was done using an Instron® model 5564 testing machine according to ASTM D 2256-90. All of the tests were performed at standard conditions of 21°C (±1°C) and 65% (±2%) relative humidity. Pneumatic yarn/cord grips were used for the yarn tests, with an effective gauge length set at 150 mm and a cross-head speed of 10%/min. Single filament tests were performed on a MTS® tester. The sample gauge length was 25 mm and the cross-head speed was also 10%/min. Griping effects were corrected by adjusting the gauge length. Initial modulus was calculated for a strain range of 0.05–0.5%, where the stress–strain curve is linear. The coefficients of variance (cv) were 1.5% in the measurement of the modulus E and 3% in the strength σ and the strain to break.

Structural characterization was carried out using wide-angle X-ray diffraction (WAXD). The structure parameters investigated include lattice constants, a, b, c; paracrystalline parameter, g_{II}; equatorial X-ray diffraction crystallinity, X; intensity ratio of the principal equatorial reflections, I_{110}/I_{200}; apparent crystal sizes (ACS) measured from the broadening of reflections from (00l), (110) and (200) planes; and (200) mis-orientation angle, ϕ_{200}.

The degree of crystallite mis-orientation, ϕ_{200}, was obtained using monochromated, pin-hole-collimated CuK_α radiation and a Bruker two-dimensional area detector. Specimens were prepared by aligning bundles under slight tension and then holding them together by epoxy resin. The applicability of this method was confirmed by agreement with that of a single filament obtained by a Statton Camera. The (200) orientation angle was taken as the full angular width at the half maximum intensity (FWHM) of the azimuthal scan of the (200) to simplify the calculation. The integrated azimuthal scan was curve-fitted using "Microcal™ Origin™" in order to calculate the integral width. According to Northolt and Aartsen [3], the (200) orientation angle represents the mis-orientation between the crystallites and the fiber axis. Five specimens for each kind of fiber sample were measured.

Other structure parameters were obtained using Ni filtered CuK_α radiation and a Siemens D500 diffractometer. Defining slits of 0.3° and a receiving slit of 0.15° was used. Corundum powder with 1 μ particle size was used as the standard sample to calibrate the angle and evaluate the

instrumental broadening. A Lorentzian profile was assumed for the peaks. The instrumental broadening was FWHM = 0.26°. Samples for diffractometry were prepared by aligning 1000 filaments and confining them into a thickness of about 100 μm. The width of the sample was 2 mm. Spectra from three specimens were collected for each fiber condition. Equatorial scans were performed using normal-transmission geometry while meridional scans were collected using $\theta/2\theta$ symmetrical-transmission geometry. The diffracted intensity distribution as a function of 2θ was first corrected for background scatter, polarization, Lorentz, and adsorption factors [21]. The polarization factor, P, used was $P = 1/2(1 + \cos^2 2\theta)$, the Lorentz factor, L, was $L = 2/\sin 2\theta$, and the adsorption factors, A, were

$$A = \frac{\exp(\mu t(1 - \sec 2\theta) - 1}{\mu t(1 - \sec 2\theta)} \quad \text{and}$$

$$A = \frac{\sec \theta}{\exp(-\mu t(1 - \sec \theta))}$$

for the normal-beam transmission and symmetrical-transmission geometries, respectively. In the above expressions θ is the Bragg angle; t the thickness of the specimen; and μ the linear absorption coefficient, calculated to be 8.43 cm^{-1}.

The c-axis lattice dimension, ACS along c, and paracrystalline parameter g_{II} were obtained from the meridional scan of the fiber. The purpose of performing this scan in $\theta/2\theta$, symmetrical transmission mode was to continually keep the fiber tilted by the Bragg angle and hence to keep it in reflecting position throughout the scan. Step/scan times were required to be such that the number of counts at the maximum intensity of one peak was above 2000. The ACS along c-axis and the paracrystalline parameter were derived using 002, 004, and 006 diffraction peaks from the following equation [22]:

$$(\delta s)_0^2 = (\delta s)_c^2 + (\delta s)_{II}^2 = I/L_{hkl}^2 + (\pi g_{II})^4 m^4 / d_{hkl}^2$$

in which δs is the broadening of the diffraction peak; L the crystal size; g_{II} the paracrystalline distortion parameter; m the order of the diffraction peak; and d_{hkl} the spacing of the first order of the diffraction plane.

Peak widths were determined using a regression analysis. While it is recognized that strictly this equation assumes Gaussian profiles for the line shapes, Voigt functions were

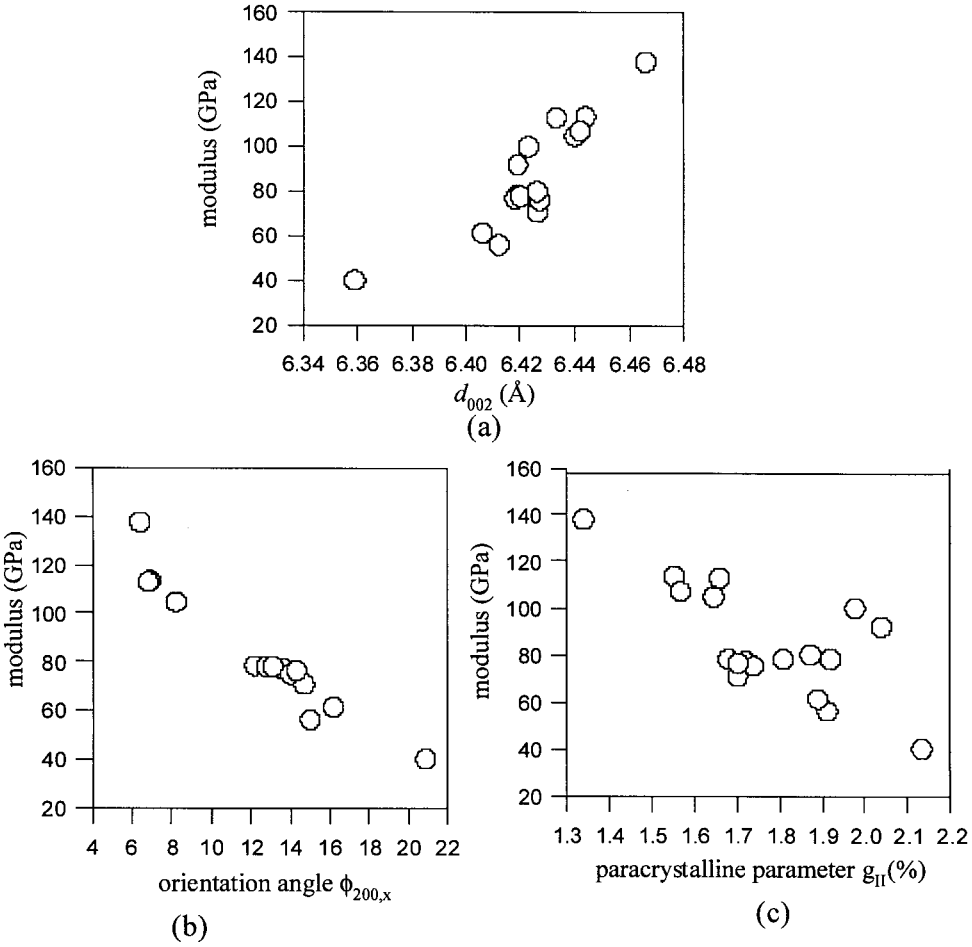

Fig. 1. Observed relationship between the initial axial modulus and different structure parameters: (a) inter-planar spacing d_{002}; (b) orientation angle $\phi_{200,x}$; (c) paracrystalline parameter g_{II}.

found to give better fits. It is not considered that this introduces sizable errors.

The *a*-, *b*-dimensions of lattice constants, ACSs from the 110 and 200 reflections, equatorial crystallinity and I_{110}/I_{200} were obtained from the equatorial scan, (performed using normal-beam transmission mode). The scanning range of 2θ was from 10 to 35°. After corrections, the intensity profile was resolved into three peaks, 110, 200 and 211 (which, because of the very large value of *c*, hence large reciprocal lattice vector, c^*, spreads some intensity from the first layer line onto the equator), and an amorphous component. Voigt functions were assumed for peaks. Then, the FWHM and the integrated intensity of the peaks were calculated. The ACSs were calculated using the Scherrer equation. The equatorial crystallinity is defined as $X = \sum I_i/(\sum I_i + I_a)$, where I_i is the integrated intensity of a diffraction peak and I_a the integrated intensity of the amorphous component.

The following table lists the statistical errors for different measurements for the structure characterization. Error bars will not be included in Section 3.

	Lattice constant (Å)	Paracrystalline parameter g_{II} (%)	Equatorial crystallinity *X* (%)	Intensity ratio I_{110}/I_{200}
Standard deviation[a]	0.003	0.04	4	0.03
	Apparent crystal size (nm)		(200) Orientation angle, (°)	
	(110), (200)	(00*l*)		
Standard deviation[a]	0.2	7	0.3	

[a] Listed numbers are the maximum standard deviation in the measurement of different samples.

3. Results and discussion

3.1. Structure–property correlation

Results showing the systematic evolution of the structure and property in PPTA fibers with post-treatment conditioning will be presented in Ref. [20]. Resultant fibers have moduli in the range of 40–138 GPa and strengths in the range of 86 MPa to 2.85 GPa. The purpose of the present paper is to develop a correlation between structure and properties using these results and to formulate a useful structural model. Correlation plots between the modulus *E* and each of the following structure parameters, *a*, *b*, *c*, g_{II}, ACS_{110}, ACS_{200}, ACS_{00l}, *X*, I_{110}/I_{200}, $\phi_{200,\,x}$ were made. Plots of *E* against *a*, *b*, ACS_{110}, ACS_{200} and ACS_{00l} all showed significant scatter, indicating the absence of any significant correlation. Results also did not show any meaningful correlation between modulus and equatorial crystallinity, in contrast to the finding of Hindeleh and Abdo [5]. In this respect, it is necessary to point out that the large experimental variability in this measurement of crystallinity precludes a precise analysis. However, it is also worthwhile to point out that the equatorial "crystallinity", as defined, does not represent total crystallinity. Nevertheless, our results suggest that a single-phase imperfect-crystalline structure describes the morphology of PPTA fiber better than a two-phase crystal/amorphous structure.

In contrast to the insensitivity of the modulus to some structure parameters, other structure parameters showed a strong effect on the modulus. Fig. 1 shows that the modulus of the fiber is related to three structure parameters: crystallite orientation, paracrystalline parameter and *c*-dimension lattice constant. There is an overall trend in that the modulus increases with decreasing mis-orientation angle and paracrystalline parameter, and with increasing *c*-dimension.

Experiments were conducted to investigate if the crystalline orientation was related to the paracrystalline parameter: however, results showed them to be independent. Our findings should be seen in the context of previous work. Northolt and Aartsen [3] proposed a correlation between modulus and orientation angle using an argument based on molecular mechanics, analogous to contemporary composite theory. Meanwhile Barton's [4] correlation of modulus with paracrystalline parameter is a phenomenological result. However, we believe that the current work represents a more comprehensive study of structure–property relationships than anything attempted previously.

During our post-treatment study, it was found that the paracrystalline parameter was particularly sensitive to post-treatment temperature while orientation was more sensitive to applied tension. This is shown in Fig. 2, which illustrates different trends in orientation angle and paracrystalline parameter with treatment temperature under different tensions.

One interesting and striking finding in our study was that

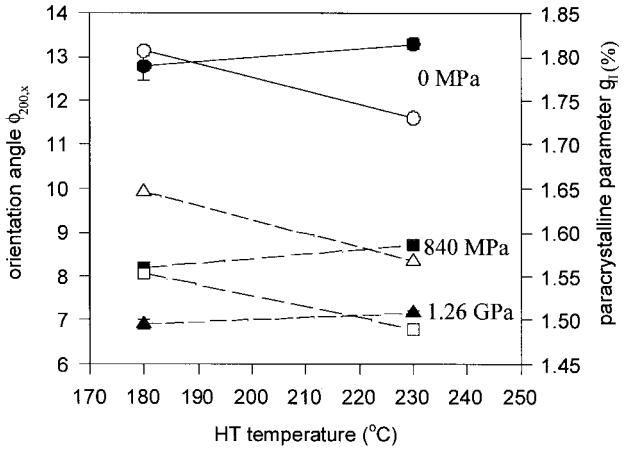

Fig. 2. Changes of the orientation (closed symbols) and paracrystalline parameter (open symbols) when fibers are subjected to elevated temperature and tension. The tensioning stresses are shown in the plot and the treatment time for zero stress is 3 h and for others is 3 min.

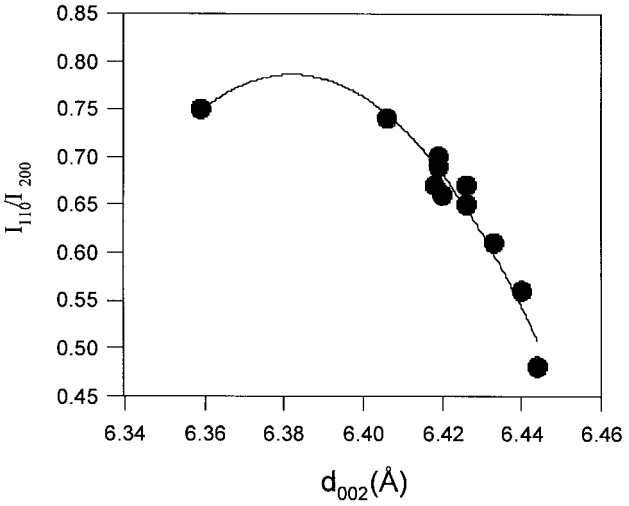

Fig. 3. Observed relationship between two structure parameters: intensity ratio I_{110}/I_{200} vs. d_{002}. The dots in the plot are experimental data and the line is a second order polynomial fitting curve.

the *c*-dimension of lattice constants differed for the fibers obtained from different post-treatment conditions. This can be understood as follows. Because the solution from which the fiber is spun is a lyotropic liquid crystal phase, the ordered, crystal structure in the fiber forms from the liquid crystal state at very high rates. This ordered structure is frozen via coagulation and is probably nonequilibrium, with chains distorted from their ideal crystal equilibrium conformations. Therefore, any post-treatment allows the chain to approach its equilibrium conformation within the crystal. This concept of the distortion of a single chain, away from its optimum comformation, will be used to derive some details of the crystal structure in the later discussion.

During our post-treatment study, it was also found that there were cooperative changes between the structure parameters c, g_{II}, and I_{110}/I_{200}. For instance, under some post-treatment conditions, when the a, b, lattice parameters remained constant, d_{002} (equal to $c/2$) and I_{110}/I_{200} followed the trend shown in Fig. 3. This clearly indicates that the I_{110}/I_{200} decreases with increasing d_{002} with I_{110}/I_{200} falling from ~0.75 to ~0.5 (Fig. 3). While the fitting is simply intuitive a second order polynomial accordingly represents the data well. The fall in the ratio of I_{110}/I_{200} is consistent with perfecting of the hydrogen bonding pattern on the *bc* plane of the lattice (hence increasing I_{200}), which is seen to be commensurate with an increase in c. Both this and the increase in c are consistent with increased lattice perfection as the chain approaches its equilibrium conformation. Some of the change in the I_{110}/I_{200} may also be possibly introduced by a change in the setting angle of phenyl groups, again caused by change in the chain conformation. It is again emphasized that this correlation only holds under the condition that the *a*-, *b*-dimensions do not change. When *a* and *b* change under post-treatment conditions the relationship shown in Fig. 3 was not followed.

However, a more general, and therefore more important, correlation between the paracrystalline parameter and the *c*-dimension was observed. As shown by Fig. 4, using the structure parameters obtained for all the fiber samples studied, a linear relation between g_{II}^2 and d_{002}^2 was found, expressed by the following equation:

$$g_{II}^2 = 87.23 - 2.04 d_{002}^2 \quad (1)$$

The basis for the correlation can be explained by the morphological and distortion model of the crystal shown by Fig. 5a. In PPTA the concept of the paracrystal [23] may be understood in terms of distortions in the PPTA chain away from strictly linear character ("nonlinear

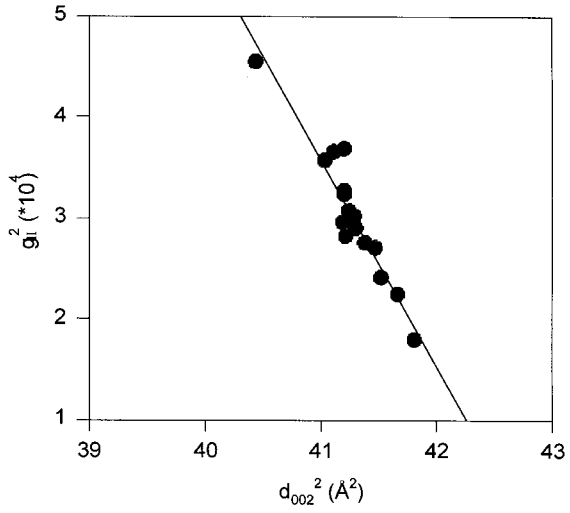

Fig. 4. Observed relationship between two structure parameters: paracrystalline parameter vs. d_{002}. The dots in the plot are experimental data and the line is a linear regression curve.

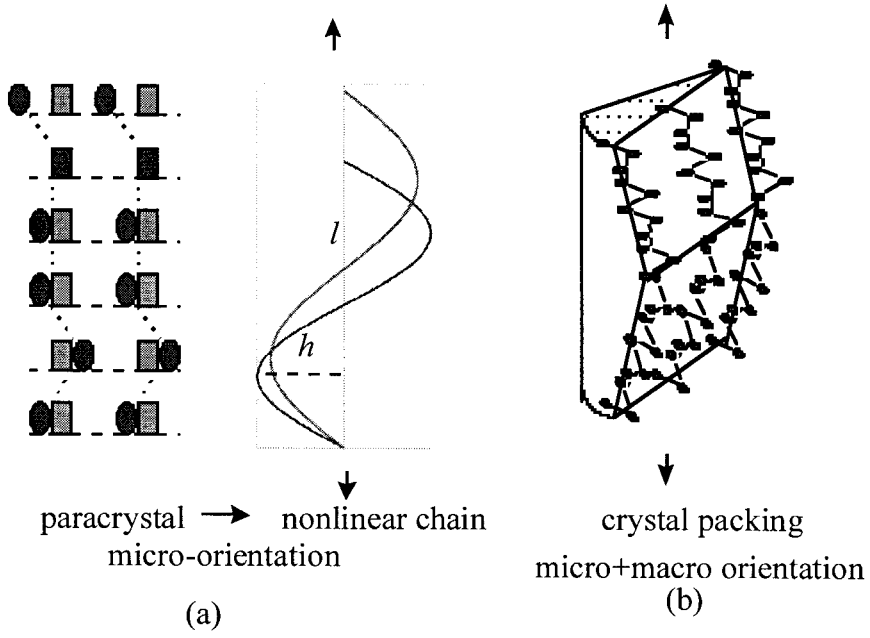

Fig. 5. A morphological model for the deformation of Kevlar® fiber: (a) a model of nonlinear chain; (b) a model of a crystallite aggregate.

chain"), hence leading to variations in repeat distances and electron-density distributions. The nonlinear chain can be treated as a sinusoidal curve.

Expressed simply, a departure from the linear conformation will have the effect of producing a contraction of the (vertical) chain projection along c and an increase in the diameter of the, admittedly irregular, helix encapsulating it. These changes are proportional provided the chain contour length is conserved. The amplitude of lateral projection can be represented by h while the degree of vertical distortion is related to g_{II}. Under any post-treatment condition, the chain conformation evolves with a change in h and l while the contour length of the chain is conserved. Under this condition, it is easy to obtain mathematically the following equation:

$$2\pi^2 h^2 + l^2 = L^2 \tag{2}$$

in which, L is the contour length of the chain in one period; and l proportional to the lattice constant along c, i.e. d_{001}.More generally, for any shape of a periodical function, the above equation becomes

$$A_1 h^2 + B_1 l^2 = C_1 L^2 \tag{3}$$

where, A_1, B_1, C_1 are constants related to the shape of the periodic function.

Eq. (3) predicts a linear relation between g_{II}^2 and d_{002}^2, which parallels the experimental observation well.

It is clear that the changes in the structure parameters d_{001}, g_{II} and I_{110}/I_{200} are interrelated. The increase in d_{001} has been correlated with decreases in g_{II} and I_{110}/I_{200}. All these three parameters are indicators of the same phenomena of crystal distortion. Our results suggest that this change in crystal structure during post-treatment is due to subtle changes in chain conformation. Moreover, the conformational changes can be related to chain deformation, (principally the lengthening of the "nonlinear" chains in the bent structure).

Furthermore, the change in the structure occurring during the post-treatment is preserved and it is this change in structure that leads to the change in the property. This structural change is related to changes in the inter-chain hydrogen bonding. It is proposed that the hydrogen bonding can be over-come at elevated temperature or under high tension and then reforms once the fiber is cooled and released from tension. Hence, the hydrogen-bonding pattern can be rearranged, resulting in removal of chain conformation distortions and an increase in lattice perfection. Releasing the tension at lower temperature prevents the relaxation of the newly formed conformation. Similar changes in the I_{110}/I_{200} have also been observed in the moisture sorption of the Kevlar® fibers [24]. It was reported that the I_{110}/I_{200} increases with the drying of the wet fiber and decreases again when the fiber regains moisture. An increase in paracrystalline parameter in the dried samples was also shown by these authors. Such results are again consistent with the formation of hydrogen bonds between PPTA amide groups and water molecules, thereby altering the details of the crystal structure.

Our morphology model is developed further as shown by Fig. 5b to construct the relation between the fiber modulus and structure. In this the finite crystallites are packed together to form a crystal aggregate with a distribution in orientation. Superimposed upon this is

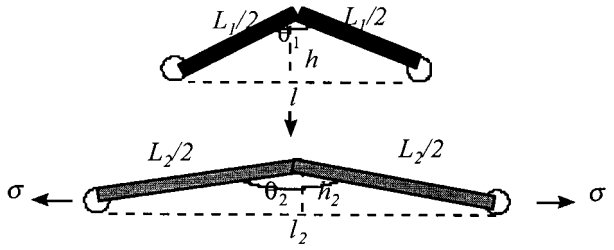

Fig. 6. Deformation of a hinged bent beam.

another source of mis-orientation as the crystallites pack into the pleated structure. Using this morphology model, a relation between the fiber modulus and the structure is derived as follows.

3.1.1. The modulus of the crystallite

To simplify the calculation, the nonlinear chain is now represented by a hinged bent beam as shown in Fig. 6. Under axial stress P, there will be bending and stretching of the structure.

Defining $\Delta\theta = \theta_1 - \theta_2$, in which θ_1 is the initial bending angle; θ_2 the final bending angle, the bending of the structure under stress σ follows

$$\Delta\theta = \tau\sigma h_2 \tag{4}$$

where σ is the applied axial stress; h_2 the deflection at the middle of the beam from the center line after loading; and τ the material constant.

Then, under loading, the total contour length becomes

$$L_2 = L_1 + L_1\sigma\sin(\theta_2/2)/E_0 \tag{5}$$

where L_1 is the initial contour length; and E_0 the Young's modulus of a linear chain. Therefore, when the $\Delta\theta$ is small ($\ll 1$), the elongation of the structure entity is

$$\epsilon = \frac{(l_2 - l)/l}{[(\Delta\theta/2)\cos(\theta_1/2) + \sigma/E_0\sin^2(\theta_1/2)]/\sin(\theta_1/2)} \tag{6}$$

Substituting $\sin(\theta_1/2) = (1 - (2h/L_1)^2)^{0.5}$ and $\cos(\theta_1/2) = 2h/L_1$, where h is the initial deflection at the middle point without load, into Eq. (6) and defining the modulus of the structure entity $E = \sigma/\epsilon$, the modulus E will be

$$E = (1 - (2h/L_1)^2)^{0.5}/[1/E_0 + (\tau/l - 4/(E_0L_1^2))h^2] \tag{7}$$

Eq. (7) can be simplified when $h \ll L_1$, and rewritten as

$$1/E = 1/E_0 + Dh^2 \tag{8}$$

where $D = (\tau/l - 4/E_0l^2)$ Eq. (8) shows that the crystallite modulus changes with the nonlinearity of the chain.

3.1.2. The modulus of the fiber

The fiber modulus is determined by the modulus of the crystallite and the orientation distribution of the crystallites

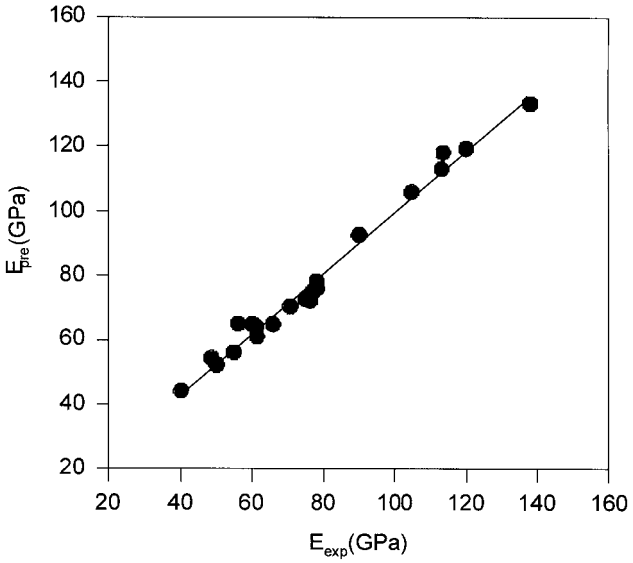

Fig. 7. A comparison of the experiment–measured modulus and the predicted modulus.

based on the aggregate model. Northolt and Aartsen's[3] equation introduced earlier is adopted to describe the effect of orientation on the modulus:

$$S_{33} = e_3^{-1} + A\langle\sin^2\phi\rangle + B\langle\sin^4\phi\rangle \tag{9}$$

This equation needs to be modified to incorporate the effect of the nonlinearity of the chain confirmation. As indicated in Fig. 5b, e_3 in Eq. (9) needs to be substituted by the crystallite modulus E expressed by Eq. (8). The combination of Eqs. (8) and (9), expressing h by g_{II} (to which it is related) and omitting the higher order term of $\langle\sin^4\phi\rangle$, yields a new equation describing the fiber modulus:

$$1/E_f = (1/E_0 + D_1g_{II}^2) + A\langle\sin^2\phi\rangle \tag{10}$$

in which, E_f is the fiber modulus; D_1 and A are the material constants. The addition of the $\langle\sin^4\phi\rangle$ term does not improve the accuracy of the expression when compared to the experimental data.

Our experimental results support our morphological model. Using Eq. (10), a least square regression was performed on the modulus and corresponding structure parameters of all different fibers, yielding good results. The regression equation is

$$1/E_f = 0.004(1 + 0.31g_{II}^2) + 0.102\times\langle\sin^2\phi\rangle \tag{11}$$

in which E_f is the fiber modulus in GPa; g_{II} the paracrystalline parameter in percent; and ϕ the orientation angle.

Fig. 7 shows the fitting is good by plotting the experimental modulus with the modulus calculated

from Eq. (11). In Eq. (11), the regression parameter A, which is 0.102, is close to the calculated value [3]. In addition, Eq. (11) yields a linear chain modulus of 250 GPa which is close to the theoretical crystal modulus [25]. Consideration of Eq. (11) indicates that the fiber modulus is dominated by orientation distribution in the low orientation region. However, to achieve ultra-high modulus, the crystallites not only need to be highly oriented, but also the nonlinearity of the chain conformation within crystallites needs to be minimized. It is apparent that, since the paracrystalline parameter is more sensitive to the post-treatment temperature while the orientation is particularly sensitive to the applied tension (as indicated earlier), the combination and control of the post-treatment condition provides a broad window to obtain fibers with different tailored properties. Clearly the modulus–structure correlation obtained for PPTA fibers can also be expected to be applicable in investigations of other rigid-rod fibers such as Technora®, Vectran® and polyimide fibers.

In addition the strength–structure relationship of different PPTA fibers was investigated; however, no general correlation was obtained. However, certain correlations did exist for fibers obtained from post-treating of one starting material, Kevlar® 29, under temperature and tension. Fig. 8 shows that the strength of the treated fiber decreased with increase in lateral crystal size. This observation is analogous to the situation encountered in metals when small crystals produce materials with high yield stress [26]. This analogy with metal systems is reasonable because PPTA also has a single-phase structure and the strength may also be determined by the packing of crystallites. Further investigation is needed to validate this suggestion.

3.2. Different types of as-received Kevlar® fibers: structure and properties

The correlation of structure with property in post-treated PPTA fibers has been discussed in Section 3.1. This correlation can also be used to explain the structural reasons for the property differences among different types of Kevlar® fibers produced by DuPont.

Table 1 compares the property and structure of different types of as-received Kevlar® fibers. It is shown that the modulus of Kevlar® 149 is 2.3 times that of Kevlar® 119, while the strength of Kevlar® 149 is 73% of that of Kevlar® 119. When comparing the modulus and strength of different types of Kevlar®, opposite trends are shown, i.e. for the modulus, Kevlar® 149 > Kevlar® 49 > Kevlar® 29 > Kevlar® while for the strength, Kevlar® 149 < Kevlar® 49 < Kevlar® 29 < Kevlar® 119.

The table clearly suggests that the structure parameters determine the difference in properties. As can be seen in the table, the orientation becomes progressively poorer from Kevlar® 149 to Kevlar® 49 to Kevlar® 29 to Kevlar® 119. In addition, the g_{II} of different fibers follows the trend that Kevlar® 149 < Kevlar® 49 < Kevlar® 29 < Kevlar® 119; the c-dimension and I_{110}/I_{200} also change systematically in accordance with our previous observations, i.e. low g_{II} is associated with large c and low I_{110}/I_{200}. It was confirmed by our data that, in the case of Kevlar® 149, both orientation and paracrystalline parameter need to be considered to explain the very high modulus.

The table also shows that the transverse crystal sizes increases from Kevlar® 119 to Kevlar® 29, to Kevlar® 49 to Kevlar® 149. This is consistent with our correlation between strength and structure. There are also other structural differences among different fibers. Although the a-, b-dimensions of Kevlar® 119, Kevlar® 29 and Kevlar® 49 are the same within experimental error, a is larger and b is smaller for Kevlar® 149 compared to the others. In addition, the axial crystal size of Kevlar® 149 is considerably larger.

In order to examine the more subtle structural differences between fibers, a synchrotron source was used. It was clear from the patterns that Kevlar® 119, Kevlar®

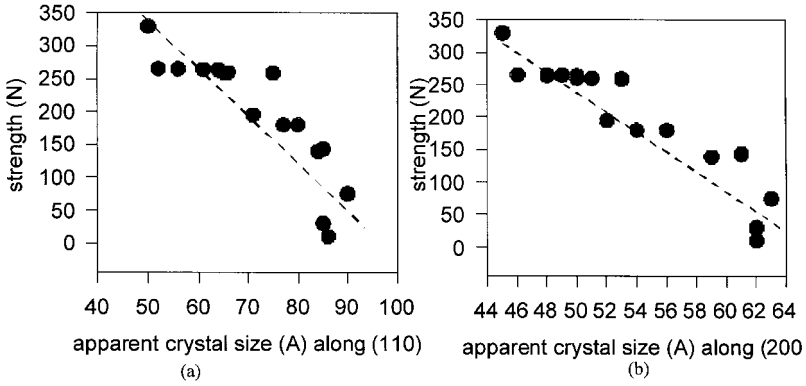

Fig. 8. The decrease in the strength of the fibers with the increasing transverse ACS for treated Kevlar® 29 fibers: (a) ACS normal to (110); (b) ACS normal to (200).

Table 1
The property and structure parameters of different types of Kevlar® fibers

		Kevlar® 119	Kevlar® 29	Kevlar® 49	Kevlar® 149
Property	Modulus (GPa)	61 ± 1	78 ± 1	113 ± 2	138 ± 2
	Tenacity (GPa)	2.96 ± 0.09	2.58 ± 0.07	2.40 ± 0.07	2.15 ± 0.06
	Breakage strain (%)	4.1 ± 0.1	3.1 ± 0.1	2.47 ± 0.1	1.5 ± 0.1
	Energy to brk. point (J)	1.27 ± 0.03	0.95 ± .03	1.23 ± .04	0.36 ± .01
Structure	Lattice constant				
	a (Å)	7.750 ± 0.003	7.748 ± 0.003	7.784 ± 0.003	7.904 ± 0.003
	b (Å)	5.224 ± 0.003	5.232 ± 0.003	5.232 ± 0.003	5.188 ± 0.003
	c (Å)	12.82 ± 0.01	12.84 ± 0.01	12.88 ± 0.01	12.92 ± 0.01
	Paracrystalline parameter g_{II} (%)	1.91 ± 0.02	1.92 ± 0.02	1.66 ± 0.04	1.40 ± 0.03
	Equatorial X-ray diffraction crystallinity X (%)	75.20	75.70	77.00	77.00
	Intensity ratio, I_{110}/I_{200}	0.74 ± 0.03	0.70 ± 0.02	0.61 ± 0.02	0.60 ± 0.02
	Apparent crystal size (nm)				
	(002)	609.19	656.14	737.15	1547.79
	(110)	50.00	52.00	66.00	123.00
	(200)	45.00	46.00	51.00	76.00
	(200) orientation angle (°)	16.2 ± 0.2	12.2 ± 0.3	6.8 ± 0.1	6.4 ± 0.2

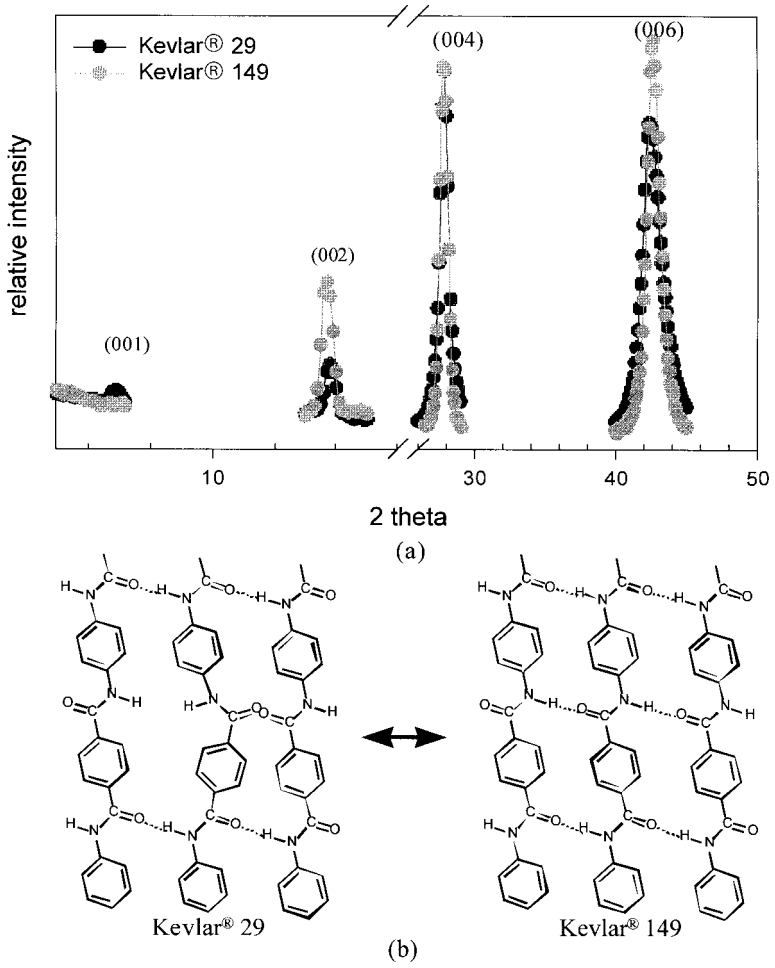

Fig. 9. The differences in WAXD profiles and suggested structural differences between Kevlar® 29 and Kevlar® 149. (a) Meridional scans; (b) suggested chain conformations in *bc* plane.

29 and Kevlar® 49 have trace diffraction intensity from the forbidden 001 diffraction peak, while in Kevlar® 149, this disappears. Fig. 9a compares the meridional scans of Kevlar® 29 and Kevlar® 149. The existence of 001 diffraction in Kevlar® 119, Kevlar® 29 and Kevlar® 49 originates from the fact that in these fibers the chain conformation does not exclusively exhibit the perfect 2_1 symmetry along *c*. However, upon heat and tensioning, *gauche*, or so-called *cis*, conformations in PPTA are transformed to the more stretched *trans* conformation as shown in Fig. 9b. In Kevlar® 149, the structure inherently has a more perfect 2_1 symmetry and the diffraction from 001 vanishes. This also promotes the formation of hydrogen bonds between chains within the *bc* plane. Therefore the number of hydrogen bonds increases and thus the *b*-dimension is also shortened. Meanwhile, the *a*-dimension is enlarged for steric reason. In addition, the change in chain conformation facilitates crystal growth along the direction of hydrogen bonding, (the *b*-axis). Therefore, the crystal size of (110) is much larger than (200) in Kevlar® 149 compared to other types of Kevlar® fibers. Clearly similar events occur during the post-treatments of the other types of Kevlar®, allowing improvements in structure shown schematically in Fig. 5a.

4. Conclusions

PPTA fibers with various properties were produced using a variety of post-treatment conditions including temperature, tension, hydrostatic pressure with environments of inert gas, water or steam. A range of different types of commercially available Kevlar® fibers were used. Mechanical properties and structure parameters were investigated for these fibers. Results show that several structure parameters change with treatment condition, indicating the structural modifications responsible for the property changes. The *c*-dimension, g_{II} and I_{110}/I_{200} are shown to be interrelated and changes in these parameters are shown to indicate irreversible chain deformation and crystal perfecting due to post-treatment. Our experimental results suggest that fiber modulus is determined by the combination of crystallite orientation and paracrystalline parameter. The correlation between structure parameters and modulus and structure parameters is confirmed by our morphological model which indicates the importance of a "local orientation" and "macro-orientation" in determining the final modulus.

The property and structure of different types of Kevlar® fibers, Kevlar® 119, Kevlar® 29, Kevlar® 49 and Kevlar® 149, were investigated. Our new structure–property correlation explains the different properties of these fibers well. Detailed diffraction studies also illustrate that the mechanism for obtaining ultra-high modulus PPTA such as Kevlar® 149 is to eliminate the "*cis*" conformation in the chain structure, thus also perfecting the order on the hydrogen-bonded sheets.

Acknowledgements

We would like to thank the E.I. DuPont Co. (USA) for the financial support for this study through the Center for the University of Massachusetts Research on Polymers (CUMIRP). Y.Q.R. thanks Prof. E.D.T. Atkins (University of Bristol) and Dr Steven R. Allen (DuPont Co.) for helpful discussion. We would also like to acknowledge the support from the Materials Research Science and Engineering Center (DMR 9809635) at University of Massachusetts and the NSLS at Brookhaven National Laboratory for use of facilities.

References

[1] Kwolek SL, US Patent, 3671542, 1972
[2] Yang HH. Kevlar aramid fiber. New York: Wiley-Intersience, 1992.
[3] Northolt MB, Aartsen JJV. J Polym Sci, Polym Symp 1977;58:283–96.
[4] Barton R. Macromol Sci Phys 1986;B24:119.
[5] Hindeleh AM, Abdo SM. Polym Commun 1989;30:184.
[6] Lee KD, Barton R, Schultz JM. J Polym Sci, Part B: Polym Phys 1995;33:1.
[7] Northolt MG, Aartson JJV. J Polym Sci, Polym Lett Ed 1973;11:333.
[8] Northolt MG. Eur Polym J 1974;10:799.
[9] Watt W, Perov BVE. Strong fibres. New York: North-Holland, 1985.
[10] Panar M, Avakian P, Blumem RC, Gardner KH, Fierke TD, Yang HH. J Polym Sci, Part B: Polym Phys 1983;21:1955.
[11] Wu T, Blackwell J. Macromolecules 1996;29:5621.
[12] Hagege R, Jarrin M, Sotton MJJ. Microscopy 1979;113:65.
[13] Riekel C, Eddola A, Heidelbach F, Wagner K. Macromolecules 1997;30:1033.
[14] Dobb MG, Johnson DJ, Saville BP. J Polym Sci, Polym Phys Ed 1977;15:2201.
[15] Konopasek L, Hearle JWS. J Appl Polym Sci 1977;21:2791.
[16] Wu Z, Zhang A, Cheng SZD. J Polym Sci, Part B: Polym Phys 1990;28:2565–83.
[17] Parimala HV, Vijayan K. J Mater Sci Lett 1993;12:99–101.
[18] Allen SR, Roche EJ, Bennett B, Molaison R. Polymer 1992;33:1849.
[19] Dupont 1972, US Patent 1,198,081.
[20] Rao Y, Waddon AJ, Farris RJ, 2001;42:5925–35.
[21] Alexander LE. X-ray diffraction methods in polymer science. New York: Wiley, 1969.
[22] Hosemann R, Wilke W. Macromol Chem 1968;118:230–49.
[23] Hosemann R, Wilke W. Faserforsch Textiledmik 1964;15:521.
[24] Fukuda M, Kawai H. J Polym Sci, Part B: Polym Phys 1997;35:1423–32.
[25] Tashiro K, Kobayashi M, Tadokoro H. Macromolecules 1977;10:413.
[26] Petch NJ. JISI 1953;173:25.